Oxygen Pressurized X-Ray Crystallography: Probing the Dioxygen Binding Site in Cofactorless Urate Oxidase and Implications for Its Catalytic Mechanism

Nathalie Colloc'h,* Laure Gabison,† Gérald Monard,‡ Muhannad Altarsha,‡§ Mohamed Chiadmi,† Guillaume Marassio,* Jana Sopkova-de Oliveira Santos,¶ Mohamed El Hajji,‖ Bertrand Castro,‖ Jacques H. Abraini,* and Thierry Prangé†

*CI-NAPS, UMR 6232–UCBN–CNRS–CEA, Centre Cyceron, 14074 Caen cedex, France; †LCRB, UMR 8015–Université Paris Descartes–CNRS, Faculté de Pharmacie, 75270 Paris cedex 06, France; ‡ECBT–UMR 7565–Université Henri Poincaré, 54506 Vandoeuvre-les-Nancy, France; §Max-Planck-Institut für Kohlenforschung, 45470 Mülheim an der Ruhr, Germany; ¶Université de Caen, UPRES-EA 2126 (CERMN)–UFR Sciences Pharmaceutiques, 14000 Caen, France; and ‖Sanofi-Aventis Recherche & Développement, 34184 Montpellier, France

ABSTRACT The localization of dioxygen sites in oxygen-binding proteins is a nontrivial experimental task and is often suggested through indirect methods such as using xenon or halide anions as oxygen probes. In this study, a straightforward method based on x-ray crystallography under high pressure of pure oxygen has been developed. An application is given on urate oxidase (UOX), a cofactorless enzyme that catalyzes the oxidation of uric acid to 5-hydroxyisourate in the presence of dioxygen. UOX crystals in complex with a competitive inhibitor of its natural substrate are submitted to an increasing pressure of 1.0, 2.5, or 4.0 MPa of gaseous oxygen. The results clearly show that dioxygen binds within the active site at a location where a water molecule is usually observed but does not bind in the already characterized specific hydrophobic pocket of xenon. Moreover, crystallizing UOX in the presence of a large excess of chloride (NaCl) shows that one chloride ion goes at the same location as the oxygen. The dioxygen hydrophilic environment (an asparagine, a histidine, and a threonine residues), its absence within the xenon binding site, and its location identical to a water molecule or a chloride ion suggest that the dioxygen site is mainly polar. The implication of the dioxygen location on the mechanism is discussed with respect to the experimentally suggested transient intermediates during the reaction cascade.

INTRODUCTION

UOX (uricase; EC 1.7.3.3) is a homotetrameric enzyme belonging to the purine degradation pathway, which catalyzes, in the presence of molecular oxygen, the hydroxylation of uric acid (*1*) to a primary intermediate that has been identified as 5-HIU (*2*) (1–3) as shown in the following scheme:

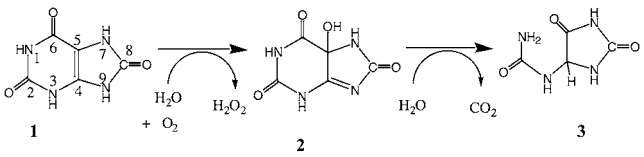

This intermediate is further transformed to S-allantoin (*3*) through a specific enzymatic cascade (4–6). UOX is present in many species but is absent in humans and higher apes. This emphasizes an evolutionary advantage: it has been suggested that uric acid is a powerful antioxidant, so humans would have less free radicals and thus less cancer as a result of aging (7,8). As a consequence, the uric acid level in plasma is quite elevated, and any higher pathological level may be lethal. The Sanofi-Aventis company produces and commercializes UOX, first extracted from *Aspergillus flavus* and now expressed in *Saccharomyces cerevisiae*, to prevent hyperuricemia that can happen during chemotherapies (9,10). The x-ray structure of UOX shows that the homotetramer is conserved in the crystal packing and presents a globular structure crossed by a tunnel 12 Å in diameter and 50 Å long (11). There are four identical active sites, each localized at interfaces between symmetrical monomers.

The catalytic mechanism of UOX does not imply any cofactor or metal ion. Several x-ray structures with or without various inhibitors have been determined to unravel the active site (12,13). Recently, the structure of the functional enzyme solved in the presence of its natural substrate, uric acid, leads to an [S]-allantoin–UOX complex showing that the enzyme has affinity for the final product of the degradation cascade (14). In the vicinity of the active site, separated by a single valine residue, is a large hydrophobic cavity where hydrophobic and anesthetic gases such as xenon or nitrous oxide specifically bind (15,16), the function of which remains unknown. Xenon is often used as a probe for dioxygen-binding sites (17,18), and it was hypothesized that the xenon binding cavity already characterized in UOX could serve for dioxy-

Submitted September 17, 2007, and accepted for publication March 12, 2008.

Address reprint requests to Dr. Nathalie Colloc'h, CI-NAPS, UMR 6232–Université de Caen Basse-Normandie–CNRS–CEA, Centre Cyceron, 14074 Caen cedex, France. Tel.: 33-2-31-47-01-32; Fax: 33-2-31-47-02-22; E-mail: colloch@cyceron.fr.

Abbreviations used: UOX, urate oxidase; 5-HIU, 5-hydroxyisourate; 8-AZA, 8-azaxanthine; FGE, formylglycine-generating enzyme; Hod, oxoquinaldine dioxygenase; Qdo, oxoquinoline dioxygenase.

Editor: Ron Elber.

0006-3495/08/09/2415/08 $2.00

doi: 10.1529/biophysj.107.122184

gen storage. In this context, we have developed a new x-ray crystallographic technique using pure oxygen under high pressure with the aim of directly localizing the dioxygen-binding site in UOX. In parallel, a structure under high concentration of NaCl, known as a good oxygen surrogate (19), was solved to confirm the usefulness of halides and xenon in probing oxygen sites.

MATERIALS AND METHODS

Purified recombinant *A. flavus* UOX, expressed in *S. cerevisiae*, and 8-AZA were supplied by Sanofi-Aventis (Montpellier, France). The crystals of the UOX/8-AZA complex were grown following the batch technique at room temperature: 10–15 mg/ml protein with an excess of 8-AZA (0.5–2 mg/ml) in 50 mM Tris/HCl, pH 8.5, in the presence of 5–8% w/v PEG 8000 and NaCl 0.05 M (20). This led to orthorhombic crystals within 24–48 h.

X-ray data collections were carried out at the BM 14 beamline (European Synchrotron Radiation Facility, Grenoble, France) at a wavelength of 0.972 Å and operating in a 16-bunch mode, using a MAR CCD detector (Evanston, IL). The temperature was set to 277 K. Crystals were mounted in a quartz capillary fitted to a specially designed pressurization cell (21,22). The cell initially designed for inert gas was adapted for the use of pure oxygen, considered as a more aggressive component (stainless steel instead of PEEK tubing). Crystals were kept under constant oxygen pressure maintained during all data collections. Three data sets were collected under oxygen pressure at 1.0 MPa, 2.5 MPa, or 4.0 MPa (10, 25, or 40 bars). No important decay of crystals was observed under dioxygen pressure, even at a pressure of 4.0 MPa, showing that at least UOX crystals can tolerate oxygen with little damage, probably because of the attenuated 16-bunch mode of the synchrotron. Data were integrated and scaled by the *HKL* package of programs (23). Cell parameters were refined by the postrefinement technique implemented in *SCALEPACK*. Final absolute data scaling was carried out with programs of the *CCP4* package (24).

A native UOX structure, the data of which were collected in the same conditions, was used as a starting model for rigid body refinement after removal of the water molecules and the ligand. Structure refinements were carried out by *REFMAC* (25) from the *CCP4* package.

Crystals of UOX have also been grown following the standard procedure previously described but with a NaCl concentration increased to 0.3 M and PEG 8000 up to 15% (w/v). In these conditions, small diamond-shaped crystals develop to their final size within a week. Data were recorded on the BM 30 Beamline (ESRF) at a wavelength of 0.963 Å. The temperature was set to 100 K. Data were integrated with *MOSFLM* (26) and then converted to structure factors and scaled as usual (24). The same reference native coordinate file previously recorded was used, after removal of all water and ligands as the starting point of the refinements, carried out with *SHELXL* (27).

The graphics program *O* (28) was used to visualize the $|2F_{obs} - F_{calc}|$, $|F_{obs} - F_{calc}|$ and omit electron-density maps and for manual refitting. A summary of the data collections and refinement statistics is shown in Table 1.

The atomic coordinates and structure factors have been deposited with the Protein Data Bank, accession numbers: 2ZKA, 2ZKB, and 3CKS for 1.0, 2.5, and 4.0 MPa oxygen pressure, respectively, and 3CKU for the structure with a chloride ion.

RESULTS

Comparison of the native UOX structure and the three structures under oxygen pressure indicates that the hydrophobic cavity, which can bind one xenon atom or two nitrous

TABLE 1 Crystallographic data collection and refinement statistics

Structure	UOX/8-AZA with oxygen			UOX/8-AZA/Cl^-
O_2 pressure (MPa)	1	2.5	4	—
Temperature (K)	277	277	277	100
Unit cell parameters (Å)				
a	80.17	79.75	80.29	78.99
b	96.23	96.29	96.15	94.98
c	105.41	105.43	105.35	104.38
Resolution range (Å)	70–1.61	70–1.61	70–1.70	70–1.70
	(1.70–1.61)	(1.70–1.61)	(1.96–1.70)	(1.79–1.70)
Unique reflections (*n*)	52,656 (5,211)	52,204 (5,133)	40,386 (4,249)	43,251 (6,302)
R_{sym} (%) overall*	5.4 (26.5)	5.5 (37.4)	5.7 (31.7)	4.7 (8.4)
Completeness (%)	99.4 (99.0)	98.8 (97.6)	89.4 (95.7)	99.6 (100)
$I/\sigma(I)$	17.0 (3.0)	11.0 (2.0)	15.0 (3.5)	22.0 (13.7)
Redundancy	4.6 (4.1)	3.4 (3.0)	3.8 (3.8)	3.5 (3.5)
Refinements				
Resolution range (Å)	15–1.61	15–1.67	15–1.70	50–1.70
R_{work} (%)†	17.2	17.1	17.1	19.3
R_{free} (%)‡	19.1	19.0	20.1	21.1
Nb of waters	217	199	181	275
Ligand and thermal *B* factor (Å^2)	O_2	O_2	O_2	Cl^-
	16.5–19.7	18.8–19.4	16.3–17.7	10.6
Weighted rmsd from ideality				
Bond length (Å)	0.011	0.013	0.012	0.035
Bond angle (°)	1.489	1.515	1.508	0.085

All structures are orthorhombic; in the I222 space group. Highest resolution shell is shown in parentheses.

*R_{sym} is defined as $\sum_{h,k,l}\sum_i |I_i(h,k,l) - \overline{I_i(h,k,l)}|/\sum_{h,k,l}\sum_i I_i(h,k,l)$ where $I_i(h,k,l)$ is the *i*th observation of reflection *h*,*k*,*l* and $\langle I(h,k,l)\rangle$ is the weighted mean of all observations (after rejection of outliers).

†R_{work} is defined as $\sum|F_o| - |F_c|/\sum|F_o|$ and indicates the accuracy of the model.

‡R_{free} is a cross validation residual calculated using 5% of the native data, which were randomly chosen and excluded from the refinement.

oxide molecules (16), remains empty whatever oxygen pressure is used, showing that dioxygen and xenon (or nitrous oxide) do not share the same binding site. The role of this large hydrophobic cavity is not then as a storage location for oxygen, although we cannot rule out a transient docking pathway for oxygen along its access to its reactive location.

The active site where inhibitors bind is located at the interface between two symmetrical monomers. In all the known UOX structures solved in the I222 space group (including 8-AZA, 9-methyl uric acid, oxonic acid, diamino-uracil, guanine (12,13), allantoin (14), xanthine, and 8-nitroxanthine (L. Gabison, T. Prangé, N. Colloc'h, M. El Hajji, B. Castro, and M. Chiadmi, unpublished data)), a water molecule called W1 is always observed, tightly hydrogen bonded to the side chains of asparagine-254 and threonine-57* from the symmetric monomer, at a distance of ~3.5 Å above the C4-C5 bond of the inhibitors (see Fig. 3 *B*). In the x-ray structure under 1.0 MPa (10 bars) oxygen pressure, when W1 is fitted within the electronic density, its resulting B-factor is lowered below 10 $Å^2$. Moreover, two residual peaks appear on both sides in the $F_{obs} - F_{calc}$ map. A dioxygen molecule, instead of W1, can better fit the omit-map density, with a full occupancy factor and resulting B-factors of ~18 $Å^2$, equivalent to those of the neighboring atoms (Fig. 1). After further refinement cycles, no residual peaks emerge from subsequent $|F_{obs} - F_{calc}|$ maps.

In the structures with 2.0 MPa (20 bars) and 4.0 MPa (40 bars) oxygen pressure, a dioxygen molecule with identical occupancy and similar B-factors is also observed at the same location, showing that dioxygen fully occupies its binding site as early as 1.0 MPa. The position of the dioxygen molecule has been optimized so that the thermal B-factors of the two oxygen atoms are of the same order (Table 1). In the three structures, the optimized refined orientation of the dioxygen molecule is slightly different. At 1.0 MPa oxygen pressure, the dioxygen leans toward the inhibitor C5 atom (angle of 109° between O_2 and C5); at 2.5 MPa oxygen pressure, the dioxygen is almost parallel to the inhibitor (angle of 83° between O_2 and C5); and at 4.0 MPa oxygen pressure, the dioxygen leans toward the inhibitor C4 atom (angle of 64° between O_2 and C5, angle of 108° between O_2 and C4). This is an indication that the dioxygen molecule is rather mobile in its binding pocket but always positioned above the C4-C5 bond of the inhibitor. In the structure with 1.0 MPa oxygen pressure, the O_2 molecule is ideally oriented for the oxidative reaction, with a distance of 3.26 Å between one of the oxygen atoms and the inhibitor C5 atom (Fig. 1). A gas pressure 10 times the physiological pressure was advocated as a necessity to saturate all binding sites in the crystal and to allow its visualization because of the crystallography technique employed (29). The structure with 1.0 MPa oxygen pressure is then likely to be the one that best represents the position of the dioxygen at ambient oxygen pressure.

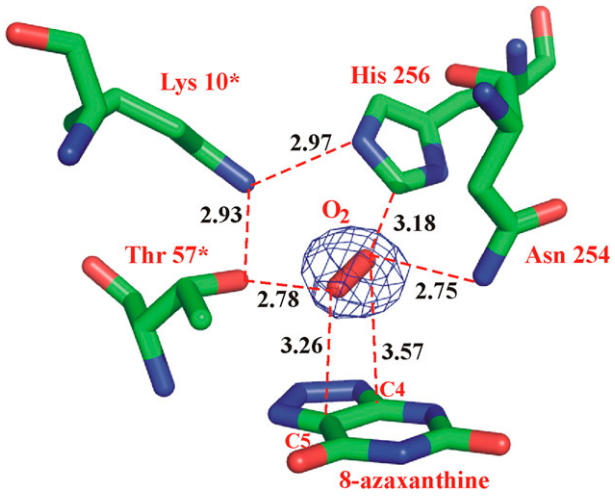

FIGURE 1 Omit map calculated by subtracting dioxygen phase contribution. The dioxygen molecule, observed here in the structure with 1.0 MPa (10 bars) oxygen pressure, is located within the active site above the inhibitor mean plane, surrounded by three conserved residues (Thr-57*, Asn-254, and His-256) (Contour levels at 3σ above the average background). This figure was produced with the visualization software *PYMOL* (DeLano Scientific, San Carlos, CA).

Carbon monoxide has been known for a long time to be a powerful inhibitor of oxygen. In a structure previously collected with 5.0 MPa pressure of carbon monoxide (data not shown), the water molecule W1 is still present, and no gas molecule can be localized either in the inert gas binding cavity or in the active site of UOX, showing that the binding site above the inhibitor remains rather specific to dioxygen.

In the structure solved at high NaCl concentration, a chloride ion is clearly observed at the location of the W1 molecule. However, the larger size of the Cl^- ion leads to a slight widening of the active site, with an elongated distance between the Asn-254 and the Thr-57* side chains (5.91 Å instead of 5.48 Å with W1 and 5.65 Å with the dioxygen molecule) and between Thr-57* and Lys-10* side chains chains (3.23 Å instead of 2.86 Å with W1 and 2.93 Å with the dioxygen molecule).

DISCUSSION

Implication in probing dioxygen-binding site

Probing dioxygen-binding sites in oxidase or heme or non-heme proteins that require molecular oxygen for their mechanism is usually investigated through indirect techniques. One of the methods consists of the use of xenon under pressure. Xenon is the prototype of a nonpolar gas, with a similar size to oxygen (4.3 Å diameter for xenon, 4.3 and 3 Å diameter for dioxygen), and it has been hypothesized that oxygen would also prefer equivalent hydrophobic environment as xenon does (17,18,30–32). It is well known that Xe-binding sites are hydrophobic cavities, often close to the active site, and have been proposed to serve as pathways or specific binding sites for molecular oxygen, as for example in myoglobin (30), cytochrome P_{450} (31), hydroxybenzoate hydroxylase (18), or copper amine oxidase (17,32). How-

ever, in the last case, because the putative oxygen-binding cavity does not bind xenon, the authors concluded that this cavity is not hydrophobic enough for xenon (17).

Recently, halide ions have also been used as dioxygen surrogates based on similar polarizability and similar volume to oxygen, with, however, different geometric criteria. This has been proposed in the case of FGE, where a small cavity beneath the disulfide-bond substrate can be occupied by a chloride, a bromide, or an iodide ion (19,33). This small cavity (32 $Å^3$) was proposed to be the oxygen-binding cavity despite its hydrophilic character (it is lined with three cysteine, serine, and tryptophan side chains plus a water molecule).

Here in UOX, we observe that oxygen under pressure does not bind the already characterized xenon (or nitrous oxide) binding cavity but is located within the active site in a polar environment, at a location usually occupied by a water molecule, above the ligand. Regarding halide ions, we observe that chloride is located at the same place as dioxygen, confirming that chloride is effectively a good candidate for probing oxygen-binding sites. Obviously, the larger size of the chloride ion and its permanent negative charge slightly modify the oxygen-binding site geometry as observed when both active site coordinates are superimposed. It is interesting to note that the polar environment of dioxygen in UOX is similar to the proposed dioxygen environment in FGE (33). These findings question the use of xenon as a specific probe for oxygen-binding sites.

We are aware that compressed oxygen could represent a highly aggressive environment, but at least in the case of UOX, because no major degradation of crystals on oxygen pressure was observed, it is believed that such an experimental approach could be extended to other biological oxidative systems because it directly evidences specific binding sites of dioxygen.

Implication for the catalytic mechanism of cofactorless UOX

The experimentally observed position of the dioxygen molecule in its specific binding site, with one oxygen atom close to the C5 atom of 8-AZA (<3.3 Å), gives new insights into the understanding of the UOX mechanism. This particular mechanism has been investigated for a long time (34) but remains interesting because this oxidase requires no cofactor or metal ion (35). In 1952, pioneering isotopic experiments showed that the oxygen atoms of hydrogen peroxide derive from dioxygen and that the oxygen atom attached to C5 in the product derives from water (34). The reaction sensitive to pH presents an optimum in basic condition (pH ~8–9). NMR studies have shown that the true product of UOX is a metastable intermediate that has been identified as 5-HIU (1–3). In addition, spectroscopic characterization of the early step of the reaction by transient-state kinetics and trapping experiments suggested that urate hydroperoxide would be an early intermediate between uric acid and 5-HIU (36).

Oxidases requiring no metal ion or prosthetic group for catalysis present the challenging problem of how molecular oxygen is activated. In cofactorless oxygenases, such as the oxoquinaldine and oxoquinoline dioxygenases (Hod and Qdo, respectively) (37), in ActVA-Orf6 mono-oxygenase whose x-ray structure has been solved (38), or in FGE (33), dioxygen and substrate activation is performed exclusively by residues of the catalytic site, probably through a direct electron transfer from the deprotonated substrate to molecular oxygen (39). It has also been suggested that they could proceed via single-electron transfer steps through a hydroperoxide intermediate (37,39,40), as for the reaction of reduced flavins and pterins with dioxygen, even if this mechanism has not been firmly established for all cases (41). UOX presents a number of similarities with pterin-binding proteins (42), and it is worth noting that their mechanisms could be related.

In the case of UOX, a step-by-step mechanism was proposed based on biochemical and x-ray diffraction experiments (36,40,43–45). In the proposed mechanism (Fig. 2), the enzyme first generates the urate dianion (*2*) from the urate monoanion (*1*) while reaching the active site. Then, the addition of dioxygen leads to 5-hydroperoxyisourate (*3*), followed by the collapse of 5-hydroperoxyisourate to lead to dehydrourate (*4*). Finally, the hydroxylation of the dehydrourate intermediate leads to 5-HIU (*5*).

The x-ray structure under oxygen pressure shows that the dioxygen molecule is localized at the same position as the W1 water molecule, confirming that the reaction proceeds following a step-by-step mechanism with implication of a hydroperoxide intermediate (*3* in Fig. 2).

In addition, we know now that the natural substrate, uric acid, occupies the same position as the different inhibitors in the active site of UOX (L. Gabison, T. Prangé, N. Colloc'h, M. El Hajji, B. Castro, and M. Chiadmi, unpublished data). We can then suggest that the di-ionic state of the natural substrate is the [$N3^-$ $N7^-$] dianion (12) (*species 2* in Fig. 2) rather than the [$N3^-$ $N9^-$] dianion as initially proposed (36). This assumption is based on the donor/acceptor complexation scheme observed on the N7/C8/O8 side of urate, where the two donors are two main-chain amido hydrogens (Fig. 3 *A*). This implies a negative charge delocalized on the N7/O8 atoms of urate. This is in agreement with quantum mechanic calculations showing that the [$N3^-$ $N7^-$] dianion once complexed has the lowest ionization potential and is the most able to give one electron to an acceptor species spontaneously (46).

The enzyme would thus need a general base to abstract the N7 proton. The structures under oxygen pressure, the already solved structures with different uric acid-like inhibitors, and the recently solved structure in the presence of uric acid do not show how the enzyme abstracts the N7 proton. We can only draw some hypothesis based on the surroundings of the substrate. Above the substrate, the water molecule W1 is tightly held by a molecular tweezers built by the side chains of two residues that belong to two different subunits, Asn-

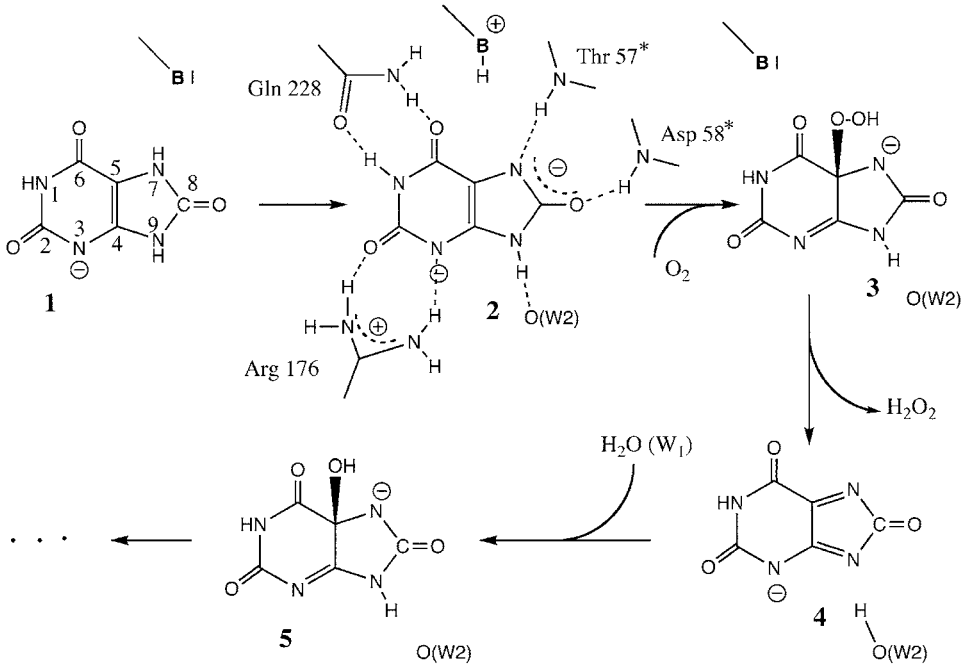

FIGURE 2 Putative urate oxidation cascade. This suggested mechanism is deduced from the active site topology based on structural results and known reported spectroscopic data.

254 and Thr-57*. In a previous study (44), the two connected residues Thr-57* and Lys-10* were mutated and found to play a role in the catalysis. In addition, the Lys-10* side chain, itself hydrogen-bonded to the His-256 side chain (Fig. 3 *B*), displays a much lower pK_a (pK_a 6.2) than usual in free solution (pK_a 10), as deduced from *PropKa* calculations (47). We can then propose that the water molecule W1, together with the Thr-57* activated by the proton relay with the Lys-10* and His-256, are implicated in the proton abstraction, even if we do not understand how, because both the W1 water molecule and the Thr-57* side chain are not in the plane of the substrate.

No mutation has yet been done to confirm the His-256 implication in the catalytic mechanism. In the cofactorless Hod, a conserved histidine was also proposed to act as a general base to generate a dianion on binding of the substrate; its mutation to an alanine leads to a drastic decrease in the catalytic activity (37). Interestingly, the UOX/Cl^- structure shows that, when a chloride ion is present in place of the dioxygen, the repulsive negative charge of the chloride abolishes the hydrogen bond between Thr-57* and Lys-10* side chains (Oδ-57*–Nζ-10* distance now increases to 3.23 Å). This suggests that chloride would also inhibit the reaction, a feature that was confirmed by kinetics experiments in high salt conditions with [NaCl] > 0.3 M (L. Gabison, unpublished results).

The second step of the reaction would consist of the dioxygen addition to lead to 5-hydroperoxyisourate (*species 3* in Fig. 2) as a transient intermediate, analogously to other cofactorless oxygenases (39). The structure of UOX under oxygen pressure clearly shows that the dioxygen molecule is ideally situated above the C4-C5 bond of the ligand (Fig. 1 and Fig. 3 *B*), ready to oxidize the dianion. The short distance between one of the dioxygen atoms and the urate C5 atom (3.26 Å) reinforces the hypothesis of an oxidation of the urate dianion at the C5 atom to yield the 5-hydroperoxyisourate, structurally confirming a hydroperoxide intermediate.

The third step of the catalysis would be the collapse of 5-hydroperoxyisourate by elimination of hydrogen peroxide to give the dehydrourate (*species 4* in Fig. 2), an analog of oxidized flavin. This compulsory-order ternary complex mechanism was already proposed in the case of Hod, where the anionic substrate binds before dioxygen, and carbon monoxide leaves the enzyme-product complex first, followed by the organic product (37).

Finally, the last step would consist of the hydroxylation of the dehydrourate intermediate to yield the final product 5-HIU (*species 5* in Fig. 2). This reaction is likely to proceed in the enzyme active site because the 5-HIU released by the enzyme is optically active (48). The water molecule W1, observed in all x-ray structures determined up to now, is perfectly positioned above the ligand and thus becomes the ideal candidate for the last step of hydroxylation (Fig. 3 *B*). In the last step, a reprotonation of 5-HIU must occur before the release of the monoanionic product. Fig. 3 *B* depicts the complete hydrogen bond network around the substrate. In this extended network, the His-256 side chain is not only hydrogen-bonded to Lys-10* but also to a water molecule (W3), itself hydrogen-bonded to the W2 water molecule. This latter molecule is always observed hydrogen-bonded to the N9 atom of the substrate (Fig. 3 *B*). Thus, the W2 molecule may be implicated in the reprotonation of the dehydrourate intermediate, leading to 5-HIU. In the absence of W2, such as in the complex of 9-methylurate (12), this protonation is abolished, which explains why 9-methyl uric acid is a competitive inhibitor of the reaction.

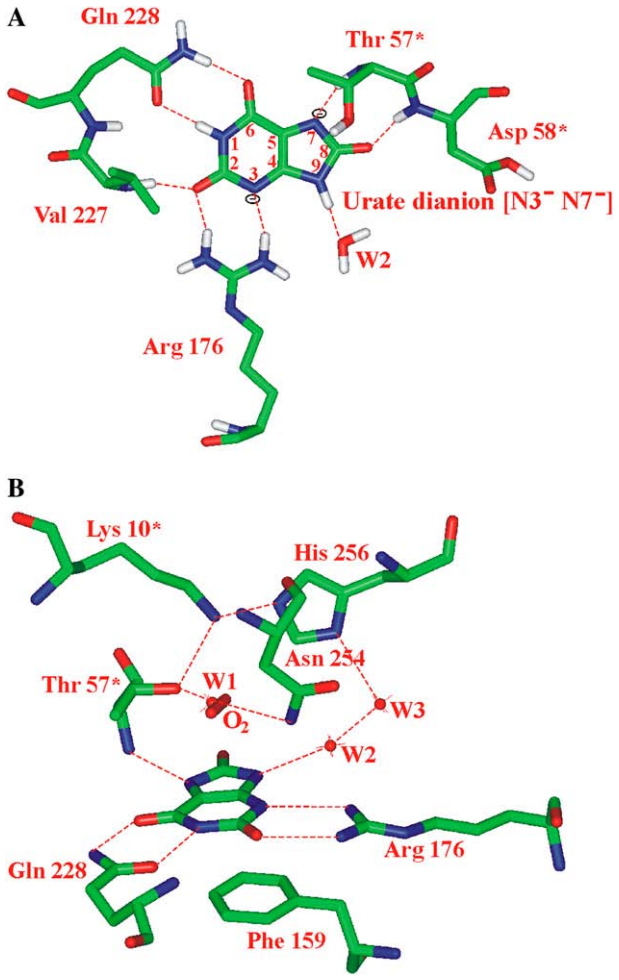

FIGURE 3 Description of the active site built at the interface of two subunits of UOX. (*A*) Because uric acid lies in the same position as uric-acid-like inhibitors, it is stacked with Phe-159 and hydrogen-bonded to the enzyme through a molecular tweezers composed by the conserved Arg-176 and Gln-228. The Val-227 is, moreover, hydrogen-bonded to the substrate through its main chain nitrogen and has its hydrophobic side chain lining the xenon-binding cavity. The five-membered ring of uric acid is linked to a symmetrical monomer of the enzyme through three hydrogen bonds: one between the N7 and the main chain NH of Thr-57*, the second between the O8 and the main chain NH of Asp-58*, and the third between the N9 and the conserved water molecule W2 (* indicates a symmetric residue). The survey of hydrogen atoms at the optimal pH of the reaction (pH 7–10) within the active site would then favor a [$N3^-$ $N7^-$] urate dianion. For clarity, only polar hydrogen atoms are displayed. (*B*) The active site showing the activated W1 molecule and the catalytic triad Thr-57*, Lys-10*, and His-256 (with W3 and W2 in relay), which can abstract a proton from the urate monoanion. The common site of W1 and the dioxygen molecule is shown above the plane of urate (W1 in hydrogen-bonded to Thr-57* and Asn-254 side chains). The hydrogen atoms are not displayed. These figures were produced with the visualization software *InsightII* (Accelrys, San Diego, CA).

Analogies with catalase

The different UOX x-ray structures support the hypothesis that the active site is designed to bind O_2 and H_2O molecules sequentially at the same location. This process is analogous to what is observed in catalase, a protective enzyme that removes hydrogen peroxide to protect cells against its deleterious effects. In mammals, catalase and UOX are colocalized in the peroxisomes of hepatic cells, where they are responsible for crystalloid core formations (49,50). Catalase also has an active site designed to bind two molecules successively at the same site: H_2O_2 then H_2O. The structure of an inactive mutant complex with H_2O_2 has shown that two H_2O_2 molecules are located immediately above the heme, at the location usually occupied in the native structure by two water molecules (51). In all known heme catalase x-ray structures, the presence and the relative orientation of a conserved His and a conserved Asn on the distal side of the heme have been highlighted (52,53). The active site on the distal side of the heme in catalase and above the uric acid in UOX shows similarities with, in both cases, a His and an Asn (see Fig. S1 in Supplementary Material, Data S1). In the x-ray structure of catalase in complex with H_2O_2 (51), one H_2O_2 molecule takes the place of the first water molecule, whereas in the x-ray structure of UOX under dioxygen pressure described here, dioxygen takes the place of W1. We can therefore suggest that, in UOX, the two conserved residues Asn-254 and His-256 are likely to play a role in binding H_2O_2. Catalase requires that H_2O_2 molecules gain a rapid access to the deeply buried active sites through a highly selective hydrophobic channel (53) while the dioxygen product exits through a separate channel (51). In the case of UOX, the dioxygen entrance and the H_2O_2 exit pathways still need to be investigated and may be different from the uric acid access channel. Moreover, the catalytic reaction of UOX in the presence of catalase is considerably accelerated by elimination of H_2O_2 (54,55). This suggests that dioxygen and then hydrogen peroxide would share sequentially a common site in UOX.

CONCLUSION

In conclusion, the structure of UOX solved under oxygen pressure demonstrates the existence of a specific polar binding site for dioxygen within the active site, above the substrate location. This site can also bind either a water molecule or a chloride ion. Moreover, oxygen does not bind within the hydrophobic xenon binding cavity previously characterized. The polar environment of oxygen questions the use of xenon as probe for oxygen-binding sites. Oxygen-pressurized x-ray crystallography might be an ideal method to localize the dioxygen site with confidence. The application to the UOX case shows that the experimentally observed oxygen molecule is ideally located above the substrate plane, ready to oxidize the urate dianion, leading to a hydroperoxide intermediate during the reaction cascade. Moreover, the location of the dioxygen molecule at the same location as the catalytic water molecule implies that the mechanism in which oxygen and water bind sequentially to a common site located above the substrate proceeds step by step. Further studies

need to be done to understand precisely how the enzyme abstracts the N7 proton to yield the [$N3^-$ $N7^-$] dianion.

SUPPLEMENTARY MATERIAL

To view all of the supplemental files associated with this article, visit www.biophysj.org.

The authors gratefully acknowledge Martin Walsh and the staff of the BM 14 beamline (ESRF, Grenoble, France) for access and advice during data collections. N.C. thanks Hélène-Marie Jouve (Institut de Biologie Structurale, Grenoble, France) for interesting discussions about similarities between catalase and UOX and Eric Girard (Institut de Biologie Structurale, Grenoble, France) for numerous discussions about the oxygen access. N.C. and J.S. also thank the CRIHAN (Rouen, France) for the use of the visualization software InsightII (Accelrys, San Diego, CA). The authors thank Arnaud Ducruix (LCRB, Paris, France) for critical reading of the manuscript.

L.G. and G.Marassio are supported by a grant from Ministère de l'Education et de la Recherche.

REFERENCES

1. Sokolic, L., N. Modric, and M. Poje. 1991. Regiochemical course of chemical and enzymic uricolysis to allantoin. A non-degradative ^{13}C-NMR evidence. *Tetrahedron Lett.* 32:7477–7480.
2. Modric, N., A. E. Derome, S. H. J. Ashcrofts, and M. Poje. 1992. Tracing and identification of uricase reaction intermediates. A direct ^{13}C-NMR/isotope-labelling evidence. *Tetrahedron Lett.* 33:6691–6694.
3. Kahn, K., P. Serfozo, and P. A. Tipton. 1997. Identification of the true product of the urate oxidase reaction. *J. Am. Chem. Soc.* 119:5435–5442.
4. Sarma, A. D., P. Serfozo, K. Kahn, and P. A. Tipton. 1999. Identification and purification of hydroxyisourate hydrolase, a novel ureide-metabolizing enzyme. *J. Biol. Chem.* 274:33863–33865.
5. Lee, Y., D. H. Lee, C. W. Kho, A. Y. Lee, M. Jang, S. Cho, C. H. Lee, J. S. Lee, P. K. Myung, B. C. Park, and S. G. Park. 2005. Transthyretin-related proteins function to facilitate the hydrolysis of 5-hydroxyisourate, the end product of the uricase reaction. *FEBS Lett.* 579:4769–4774.
6. Lee, Y., B. C. Park, H. Lee do, K. H. Bae, S. Cho, C. H. Lee, J. S. Lee, P. K. Myung, and S. G. Park. 2006. Mouse transthyretin-related protein is a hydrolase which degrades 5-hydroxyisourate, the end product of the uricase reaction. *Mol. Cells.* 22:141–145.
7. Ames, B. N., R. Cathcart, E. Schwiers, and P. Hochstein. 1981. Uric acid provides an antioxidant defense in humans against oxidant- and radical-caused aging and cancer: a hypothesis. *Proc. Natl. Acad. Sci. USA.* 78:6858–6862.
8. Wu, X. W., D. M. Muzny, C. C. Lee, and C. T. Caskey. 1992. Two independent mutational events in the loss of urate oxidase during hominoid evolution. *J. Mol. Evol.* 34:78–84.
9. Legoux, R., B. Delpech, X. Dumont, J. C. Guillemot, P. Ramond, D. Shire, D. Caput, P. Ferrara, and G. Loison. 1992. Cloning and expression in *Escherichia coli* of the gene encoding *Aspergillus flavus* urate oxidase. *J. Biol. Chem.* 267:8565–8570.
10. Bayol, A., J. Capdevielle, P. Malazzi, A. Buzy, M. C. Bonnet, N. Colloc'h, J. P. Mornon, D. Loyaux, and P. Ferrara. 2002. Modification of a reactive cysteine explains differences between rasburicase and Uricozyme, a natural *Aspergillus flavus* uricase. *Biotechnol. Appl. Biochem.* 36:21–31.
11. Colloc'h, N., M. El Hajji, B. Bachet, G. L'Hermite, M. Schiltz, T. Prangé, B. Castro, and J. P. Mornon. 1997. Crystal structure of the protein drug urate oxidase-inhibitor complex at 2.05 Å resolution. *Nat. Struct. Biol.* 4:947–952.
12. Retailleau, P., N. Colloc'h, D. Vivarès, F. Bonneté, B. Castro, M. El Hajji, J. P. Mornon, G. Monard, and T. Prangé. 2004. Complexed and ligand-free high-resolution structures of urate oxidase (Uox) from *Aspergillus flavus*: a reassignment of the active-site binding mode. *Acta Crystallogr.* D60:453–462.
13. Retailleau, P., N. Colloc'h, D. Vivarès, F. Bonneté, B. Castro, M. El Hajji, and T. Prangé. 2005. Urate oxidase from *Aspergillus flavus*: new crystal-packing contacts in relation to the content of the active site. *Acta Crystallogr.* D61:218–229.
14. Gabison, L., M. Chiadmi, N. Colloc'h, B. Castro, M. El Hajji, and T. Prangé. 2006. Recapture of [S]-allantoin, the product of the two-step degradation of uric acid, by urate oxidase. *FEBS Lett.* 580:2087–2091.
15. Prangé, T., M. Schiltz, L. Pernot, N. Colloc'h, S. Longhi, W. Bourguet, and R. Fourme. 1998. Exploring hydrophobic sites in proteins with xenon or krypton. *Proteins.* 30:61–73.
16. Colloc'h, N., J. Sopkova-de Oliveira Santos, P. Retailleau, D. Vivarès, F. Bonneté, B. Langlois d'Estaintot, B. Gallois, A. Brisson, J. J. Risso, M. Lemaire, T. Prangé, and J. H. Abraini. 2007. Protein crystallography under xenon and nitrous oxide pressure: comparison with in vivo pharmacology studies and implications for the mechanism of inhaled anesthetic action. *Biophys. J.* 92:217–224.
17. Duff, A. P., D. M. Trambaiolo, A. E. Cohen, P. J. Ellis, G. A. Juda, E. M. Shepard, D. B. Langley, D. M. Dooley, H. C. Freeman, and J. M. Guss. 2004. Using xenon as a probe for dioxygen-binding sites in copper amine oxidases. *J. Mol. Biol.* 344:599–607.
18. Hiromoto, T., S. Fujiwara, K. Hosokawa, and H. Yamaguchi. 2006. Crystal structure of 3-hydroxybenzoate hydroxylase from *Comamonas testosteroni* has a large tunnel for substrate and oxygen access to the active site. *J. Mol. Biol.* 364:878–896.
19. Roeser, D., B. Schmidt, A. Preusser-Kunze, and M. G. Rudolph. 2007. Probing the oxygen-binding site of the human formylglycine-generating enzyme using halide ions. *Acta Crystallogr.* D63:621–627.
20. Bonneté, F., D. Vivarès, C. Robert, and N. Colloc'h. 2001. Interactions in solution and crystallization of *Aspergillus flavus* urate oxidase. *J. Cryst. Growth.* 232:330–339.
21. Schiltz, M., T. Prangé, and R. Fourme. 1994. On the preparation and x-ray data collection of isomorphous xenon derivatives. *J. Appl. Cryst.* 27:950–960.
22. Schiltz, M., R. Fourme, and T. Prangé. 2003. Use of noble gases xenon and krypton as heavy atoms in protein structure determination. *Methods Enzymol.* 374:83–119.
23. Otwinowski, Z., and W. Minor. 1997. Processing of x-ray diffraction data collected in the oscillation mode. *Methods Enzymol.* 276:307–326.
24. Collaborative Computational Project Number 4. 1994. The *CCP4* suite: programs for protein crystallography. *Acta Crystallogr.* D50:760–763.
25. Murshudov, G. N., A. A. Vagin, and E. J. Dodson. 1997. Refinement of macromolecular structures by the Maximum-Likelihood method. *Acta Crystallogr.* D53:240–255.
26. Leslie, A. G. 2006. The integration of macromolecular diffraction data. *Acta Crystallogr.* D62:48–57.
27. Sheldrick, G. M., and T. R. Schneider. 1997. SHELXL: High-resolution refinement. *Methods Enzymol.* 227:319–343.
28. Jones, T. A., J. Y. Zou, S. W. Cowan, and M. Kjeldgaard. 1991. Improved methods for building protein models in electron density maps and the location of errors in these models. *Acta Crystallogr. A.* 47:110–119.
29. Miller, K. W. 2002. The nature of sites of general anaesthetic action. *Br. J. Anaesth.* 89:17–31.
30. Tilton, R. F., Jr., I. D. Kuntz, Jr., and G. A. Petsko. 1984. Cavities in proteins: structure of a metmyoglobin-xenon complex solved to 1.9 Å. *Biochemistry.* 23:2849–2857.
31. Wade, R. C., P. J. Winn, I. Schlichting, and Sudarko. 2004. A survey of active site access channels in cytochromes P450. *J. Inorg. Biochem.* 98:1175–1182.

32. Lunelli, M., M. L. Di Paolo, M. Biadene, V. Calderone, R. Battistutta, M. Scarpa, A. Rigo, and G. Zanotti. 2005. Crystal structure of amine oxidase from bovine serum. *J. Mol. Biol.* 346:991–1004.

33. Roeser, D., A. Preusser-Kunze, B. Schmidt, K. Gasow, J. G. Wittmann, T. Dierks, K. von Figura, and M. G. Rudolph. 2006. A general binding mechanism for all human sulfatases by the formylglycine-generating enzyme. *Proc. Natl. Acad. Sci. USA.* 103:81–86.

34. Bentley, R., and A. Neuberger. 1952. The mechanism of the action of uricase. *Biochem. J.* 52:694–699.

35. Kahn, K., and P. A. Tipton. 1997. Kinetic mechanism and cofactor content of soybean root nodule urate oxidase. *Biochemistry.* 36:4731–4738.

36. Kahn, K., and P. A. Tipton. 1998. Spectroscopic characterization of intermediates in the urate oxidase reaction. *Biochemistry.* 37:11651–11659.

37. Frerichs-Deeken, U., K. Ranguelova, R. Kappl, J. Huttermann, and S. Fetzner. 2004. Dioxygenases without requirement for cofactors and their chemical model reaction: compulsory order ternary complex mechanism of 1*H*-3-hydroxy-4-oxoquinaldine 2,4-dioxygenase involving general base catalysis by histidine 251 and single-electron oxidation of the substrate dianion. *Biochemistry.* 43:14485–14499.

38. Sciara, G., S. G. Kendrew, A. E. Miele, N. G. Marsh, L. Federici, F. Malatesta, G. Schimperna, C. Savino, and B. Vallone. 2003. The structure of ActVA-Orf6, a novel type of monooxygenase involved in actinorhodin biosynthesis. *EMBO J.* 22:205–215.

39. Fetzner, S. 2002. Oxygenases without requirement for cofactors or metal ions. *Appl. Microbiol. Biotechnol.* 60:243–257.

40. Sarma, A. D., and P. A. Tipton. 2000. Evidence for urate hydroperoxide as an intermediate in the urate oxidase reaction. *J. Am. Chem. Soc.* 112:11252–11253.

41. Massey, V. 1994. Activation of molecular oxygen by flavins and flavoproteins. *J. Biol. Chem.* 269:22459–22462.

42. Colloc'h, N., A. Poupon, and J. P. Mornon. 2000. Sequence and structural features of the T-fold, an original tunnelling building unit. *Proteins.* 39:142–154.

43. Tipton, P. A. 2002. Urate oxidase: single-turnover stopped-flow techniques for detecting two discrete enzyme-bound intermediates. *Methods Enzymol.* 354:310–319.

44. Imhoff, R. D., N. P. Power, M. J. Borrok, and P. A. Tipton. 2003. General base catalysis in the urate oxidase reaction: evidence for a novel Thr-Lys catalytic diad. *Biochemistry.* 42:4094–4100.

45. Doll, C., A. F. Bell, N. Power, P. J. Tonge, and P. A. Tipton. 2005. Procatalytic ligand strain. Ionization and perturbation of 8-nitroxanthine at the urate oxidase active site. *Biochemistry.* 44:11440–11446.

46. Altarsha, M., G. Monard, and B. Castro. 2007. Comparative semiempirical and ab initio study of the structural and chemical properties of uric acid and its anions. *Int. J. Quantum Chem.* 107:172–181.

47. Li, H., A. D. Robertson, and J. H. Jensen. 2005. Very fast empirical prediction and rationalization of protein pKa values. *Proteins.* 61: 704–721.

48. Tipton, P. A. 2006. Urate to allantoin, specifically (S)-allantoin. *Nat. Chem. Biol.* 2:124–125.

49. Gould, S. J., G. A. Keller, and S. Subramani. 1988. Identification of peroxisomal targeting signals located at the carboxy terminus of four peroxisomal proteins. *J. Cell Biol.* 107:897–905.

50. Alvares, K., R. J. Widrow, G. M. Abu-Jawdeh, J. V. Schmidt, A. V. Yeldandi, M. S. Rao, and J. K. Reddy. 1992. Rat urate oxidase produced by recombinant baculovirus expression: formation of peroxisome crystalloid core-like structures. *Proc. Natl. Acad. Sci. USA.* 89:4908–4912.

51. Melik-Adamyan, W., J. Bravo, X. Carpena, J. Switala, M. J. Maté, I. Fita, and P. C. Loewen. 2001. Substrate flow in catalases deduced from the crystal structures of active site variants of HPII from *Escherichia coli*. *Proteins.* 44:270–281.

52. Gouet, P., H. M. Jouve, and O. Dideberg. 1995. Crystal structure of *Proteus mirabilis* PR catalase with and without bound NADPH. *J. Mol. Biol.* 249:933–954.

53. Putnam, C. D., A. S. Arvai, Y. Bourne, and J. A. Tainer. 2000. Active and inhibited human catalase structures: ligand and NADPH binding and catalytic mechanism. *J. Mol. Biol.* 296:295–309.

54. Vogels, G. D., and C. Van der Drift. 1976. Degradation of purines and pyrimidines by microorganisms. *Bacteriol. Rev.* 40:403–468.

55. Bergmann, F., H. Ungar-Waron, and H. Kwietny-Govrin. 1963. Thiouric acids as substrates and inhibitors of mammalian urate oxidase. *Biochem. J.* 86:292–298.